Physica B 500 (2016) 4–8

Contents lists available at ScienceDirect

Physica B

journal homepage: www.elsevier.com/locate/physb

Cu_2O quantum dots emitting visible light grown by atomic layer deposition

Min Young Lee [a], Soo-Hyun Kim [a,*], Il-Kyu Park [b,*]

[a] School of Materials Science & Engineering, Yeungnam University, Gyeongbuk 712-749, South Korea
[b] Department of Materials Science and Engineering, Seoul National University of Science and Technology, Seoul 139-743, South Korea

ARTICLE INFO

Article history:
Received 11 July 2016
Received in revised form
19 July 2016
Accepted 20 July 2016
Available online 21 July 2016

Keywords:
Cu_2O
Quantum dots
Atomic layer deposition
Quantum confinement effect

ABSTRACT

This paper reports the fabrication of the Cu_2O quantum dots (QDs) emitting a controlled wavelength in the visible spectral range prepared by atomic layer deposition (ALD). Cu_2O thin film layers formed on the Al_2O_3 surface showed large density of islands via Volmer–Weber growth mode, which resulting in QD formation. As the number of ALD cycles was increased from 60 to 480, the spatial density and mean diameter of the Cu_2O QDs increased systematically from $4.02 \times 10^{11}/cm^2$ to $2.56 \times 10^{12}/cm^2$ and from 2.1 to 3.2 nm, respectively. The absorption spectral results indicated that the electron energy transition in the Cu_2O QDs was a direct process with the optical band gaps decreasing from 2.71 to 2.15 eV with increasing QD size from 2.1 to 3.2 nm because of the quantum confinement effect. The Cu_2O QDs showed broad emission peaks composed of multiple elementary emission spectra corresponding to the Cu_2O QD ensembles with a different size distribution. As the size of Cu_2O QDs decreased, the shoulder peaks at the higher energy side developed due to the quantum confinement effect.

1. Introduction

Semiconductor low-dimensional structures, such as quantum wells, quantum wires and quantum dots (QDs) have attracted considerable attention because of their importance as functional building blocks, offering unprecedented opportunities for novel device applications as well as for investigating many novel quantum phenomena [1,2]. Most studies have focused on II–VI semiconductors, such as CdS, CdSe and PbSe [3–5]. Recently, cuprous oxide (Cu_2O) nanostructures have received considerable interest because of their remarkable physical properties, such as large exciton binding energy of 140 meV, exhibiting typical excitonic features [6] and a forbidden electric dipole transition between the lowest energy of the conduction band and the top of the valence band due to the same parity [7,8]. In addition, it is a *p*-type transition metal oxide compound semiconductor that provides novel electron-correlations for superconducting and ferromagnetic physical phenomena [9]. Therefore, Cu_2O is an excellent candidate for applications in photo-voltaics [10,11], photo-catalysts [12], magnetic storage [13], gas sensor [14], and biosensors [15]. In addition, nano-structured Cu_2O has been investigated widely because of their novel optical and structural properties [8,16–18]. On the other hand, few have reported the fabrication of well-defined Cu_2O quantum structures because Cu_2O has an extremely small bulk Bohr exciton binding radius of 0.7 nm [8]. The difficulties in controlling the size, composition and matrix have limited studies on controllable quantum effects. Furthermore, the fabricated Cu_2O quantum structures are in the form of nano-powders [8,16–18], which are difficult to apply to various devices, and the shape and position of the nanostructures are difficult to control. For more compatible applications of Cu_2O QDs to other devices, the fabrication process needs to be controllable and it should be possible for the nanostructures to be fabricated on a range of substrates. This paper reports the controllable fabrication of the Cu_2O QDs on a silicon (Si) substrate by atomic layer deposition (ALD) to investigate the quantum size effect.

2. Experimental

2.1. Deposition of Cu_2O quantum dots

The Cu_2O QDs were deposited on Si (100) and sapphire (0001) substrates by atomic layer deposition (ALD) using a traveling-wave-type ALD reactor (Lucida D100, NCD Technology, Korea), which is a particularly effective method for synthesizing QDs uniformly and precisely by controlling the number of ALD cycles. Bis(1-dimethylamino-2-methyl-2-butoxy)copper ($C_{14}H_{32}N_2O_2Cu$) and water vapor (H_2O) were used as the precursor and reactant,

* Corresponding authors.
E-mail addresses: soohyun@ynu.ac.kr (S.-H. Kim), pik@seoultech.ac.kr (I.-K. Park).

http://dx.doi.org/10.1016/j.physb.2016.07.025
0921-4526/

respectively. The Cu precursor was vaporized in a bubbler at 80 °C and carried to the process chamber by N_2 gas at a flow rate of 200 sccm. Water vapor prepared in a canister kept at 10 °C was flowed into the chamber without a carrier gas. The temperature and pressure of the reactor were maintained at 140 °C and ~1 Torr, respectively. The basic pulsing conditions for Cu_2O QDs were as follows: precursor pulse for 5 s, reactant pulse for 5 s, and purge for 10 s, which were found to be sufficient to guarantee self-limited growth of the Cu_2O film. The sequence of the precursor pulse, purge, reactant pulse, and purge occurred in each ALD cycle. Immediately after forming the Cu_2O-QDs, ALD-Al_2O_3 was deposited on them *in-situ* at the same temperature. Al_2O_3 ALD was then performed using a sequential supply of trimethylaluminum [TMA, $(CH_3)_3Al$] and water vapor. TMA was contained at 10 °C and provided without a carrier gas. One ALD unit cycle for Al_2O_3 consisted of a TMA (0.2 s) pulse – N_2 purge (10 s) – H_2O pulse (0.2 s) – N_2 purge (10 s). The deposition of the Cu_2O QDs and Al_2O_3 was repeated 5 times.

2.2. Characterizations

The structural properties of the Cu_2O QDs were examined according to the number of ALD cycles by transmission electron microscopy (TEM, Tecnai F20 equipped with a 200 kV accelerating voltage and a field emission gun). Plan-view TEM analysis was used to observe the formation of Cu_2O QDs according to the number of ALD cycles and those crystalline structures. The plan-view TEM sample was prepared using conventional procedures, such as tripod polishing and Ar-ion milling. A Gatan precision ion polishing system was used for Ar-ion milling. X-ray diffraction (GIAXRD, PANalytical X'-pert MRD with Cu-K_α radiation at 1.5 kW) was performed for the phase and crystallinity identifications of the ALD deposited Cu_2O, grazing-incidence angle (incident angle, $\theta=3°$). The optical properties of the Cu_2O QDs were examined using a photoluminescence (PL) and UV-visible spectrophotometer (Scinco, S-3100). PL was performed at room temperature using a 325 nm continuous He-Cd laser with an excitation power of 27 mW.

3. Results and discussion

Fig. 1 shows GIAXRD pattern of the Cu_2O films deposited on Si (100) substrate with 2000 ALD cycles to examine the composition and crystalline structure of the deposited thin layers. The GIAXRD results of the Cu_2O film showed 5 specific peaks corresponding to cubic Cu_2O. No peak related to CuO or Cu was observed. The Cu_2O thin films deposited via same reaction condition showed very pure and stoichiometric (the ratio of Cu and O ~2:1.1) phase [19]. Hence, the film deposited at this temperature was considered to consist of pure Cu_2O.

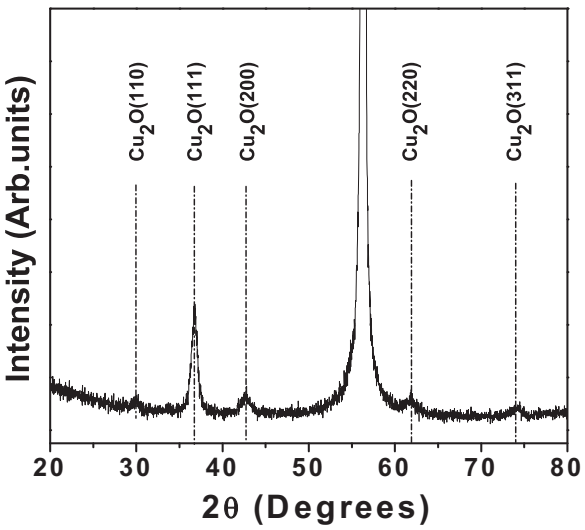

Fig. 1. GIAXRD patterns of the ALD-Cu_2O films deposited with 2000 ALD cycles.

Fig. 2(a)–(d) show the plan-view bright-field TEM images of ALD-Cu_2O for various numbers of ALD cycles of 60, 120, 240, and 480, respectively. Cu_2O QDs was observed at 60 ALD cycles, as shown in Fig. 2(a), and the QD density increased with increasing the number of ALD cycles up to 120 [Fig. 2(b)] and the QDs size increased slightly. When the number of ALD cycles was increased to 240 [Fig. 2(c)], the QDs size and their density increased continuously, even though the electron diffraction pattern (the inset figure) was quite dim, indicating the relatively low density of crystalline Cu_2O QDs. Fig. 2(d) shows that the QD size and density increased significantly with increasing the number of ALD cycles up to 480, and a high density of QDs was clearly observed in the low-magnification TEM image. As the number of ALD cycles was increased from 60 to 120, 240 and 480, the diameter of the Cu_2O QDs increased from 2.1 to 2.3, 2.9 and 3.2 nm, respectively. The selected area electron diffraction (the inset figure) clearly indicated a spotty-pattern from the cuprous Cu_2O QDs with a cubic structure (lattice parameter: 4.2696 Å and space group: $Pn\bar{3}m$). Interestingly, most Cu_2O QDs were still separated from each other, as observed in the magnified image (the inset figure of yellow box), indicating that partial coalescence of the QDs did not occur. The arrows in the figures correspond to the Cu_2O QD regions.

Fig. 3 presents a summary of the spatial density and mean diameter of the Cu_2O QDs as a function of the number of ALD cycles, which were measured from the corresponding plan-view TEM images in Fig. 2. As the number of ALD cycles increased from 60 to 480, the spatial density and mean diameter of the Cu_2O QDs increased continuously from $4.02\times10^{11}/cm^2$ to $2.56\times10^{12}/cm^2$ and from 2.1 to 3.2 nm, respectively. This behavior is usually observed behavior in the QD hetero-structures grown via Volmer–Weber growth mode because the Cu_2O atoms bound more strongly to each other than to substrate. In addition, by growing at low temperature at 140 °C, the surface diffusion of adatoms is suppressed to result in simultaneous increase of the size and density of QDs with increasing the deposit. An extrapolation of the size and density in Fig. 3 to zero growth time (number of cycles) resulted in a non-zero structure with a density of around few $10^{11}/cm^2$. In general, a zero or below-zero fitting of the diameter and the density would be expected in Stranski–Krastanov growth mode [20]. On the other hand, these results showed that Cu_2O growth is initiated with three-dimensional islands on Al_2O_3 without the formation of a wetting layer, indicating that the growth mode is assumed to be a Volmer–Weber growth mode because of a low surface energy of the Al_2O_3 layers.

Fig. 4 shows the absorption spectral results obtained by measuring a UV-visible absorption spectrometer. For the optical measurements, samples were deposited on both side polished sapphire substrates. According to the Tauc relationship, for photon energies (E, h_ν) greater than the band gap, light absorption can be approximated using [21]:

$$\alpha h\nu = \alpha_o(h\nu - E_g)^\eta$$

where h is Planck's constant, ν is the frequency of a photon, α is the absorption coefficient, α_o is a constant, and E_g is the band gap. The exponential factor, η, depends on the type of transition involved; 0.5 or 2 for a direct or indirect transition, respectively [21]. As shown in Fig. 4, the plot of $(\alpha h\nu)^2$ versus $h\nu$ was fitted well and the optical band gap was determined by extrapolating the linear

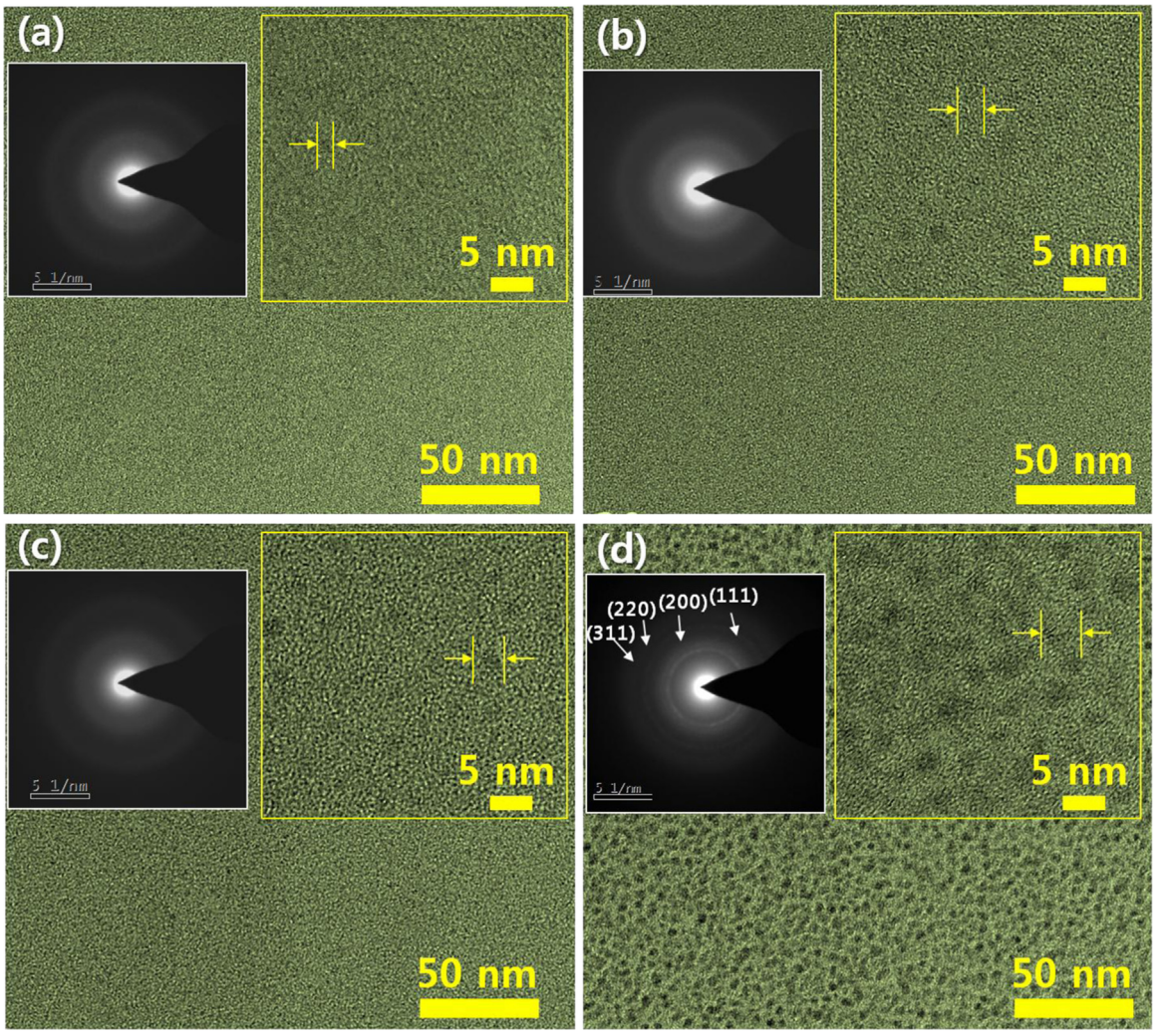

Fig. 2. Plan-view bright-field TEM images of ALD-Cu_2O for various numbers of ALD cycles; (a) 60 cycles, (b) 120 cycles, (c) 240 cycles, and (d) 480 cycles. The insets of each figure show the SAED patterns indicating the crystalline structures and magnified images to clearly show the Cu_2O QDs in each sample. And the yellow arrows correspond to Cu_2O QD regions.

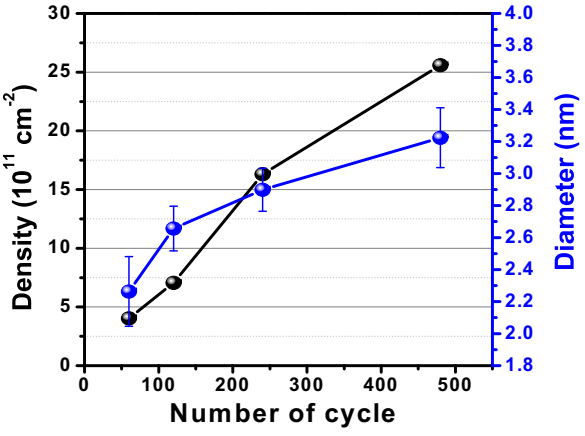

Fig. 3. Summary of the density and size of the Cu_2O QDs measured by TEM.

region of the abruption spectrum because Cu_2O is a direct band gap semiconductor. The optical absorption revealed a continuous increase, not sharp absorption features, which would be due partially to the broad size distribution of the Cu_2O QDs. The optical band gaps for the Cu_2O QDs with 2.1, 2.3, 2.9, and 3.2 nm decreased from 2.71 to 2.41, 2.23 and 2.15 eV, respectively. The

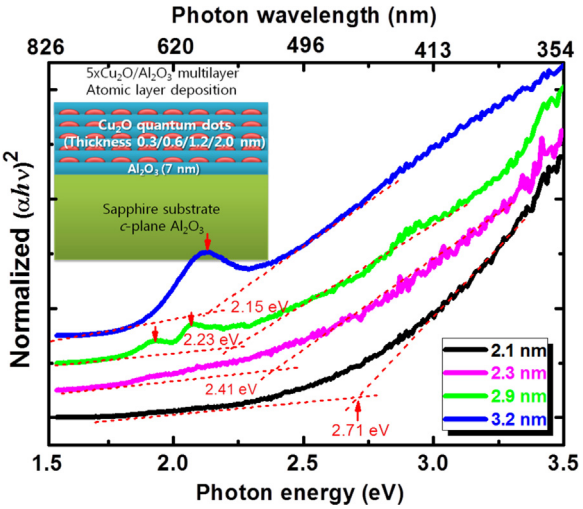

Fig. 4. Variation of $(\alpha h\nu)^2$ as a function of the photon energy ($h\nu$) to obtain the direct band gap of Cu_2O QDs with various sizes. The inset shows the schematic diagram of the sample structure of Cu_2O QDs/Al_2O_3 multiple layers deposited by the ALD system.

measured optical band gaps were 0.54, 0.24, and 0.06 eV larger for the 2.1, 2.3, and 2.9 nm Cu_2O QDs, respectively, than the bulk band gap energy (2.17 eV) of the Cu_2O materials. This large blue-shift in the band gap energy can be attributed to the size-dependent electronic transitions in the Cu_2O QDs, as suggested by the quantum confinement effect. Based on an effective mass approximation with a Coulomb interaction, the energy band gap of the Cu_2O QDs (E_{QD}) can be estimated as follows [22,23]:

$$E_{QD} = E_g + \frac{h^2}{8r^2}\left(\frac{1}{m_e^*} + \frac{1}{m_h^*}\right) - \frac{1.8e^2}{4\pi\varepsilon_r\varepsilon_0 r}$$

where E_{QD} and E_g are the lowest excitation energy of the Cu_2O QDs and the bandgap of bulk Cu_2O (2.17 eV), respectively, r is the radius of the Cu_2O QDs, h is Planck's constant, m_e^* is the electron effective mass of $0.98m_o$ [24], m_h^* is the hole effective mass of $0.66m_o$ [25], e the is electron unit charge, ε_r is the relative permittivity of Cu_2O of 7.5 [26], and ε_0 is the vacuum permittivity. The band gaps estimated by this effective mass approximation for the Cu_2O QDs with a size range between 2.1 and 3.2 nm were in the range, 2.9 and 2.3 eV. Although many parameters, such as the electrical parameters and the energy band structures of the Cu_2O materials, in this calculation were approximated, the band gap of the Cu_2O QD matched well with the experimental results. The exciton Bohr radius of the Cu_2O is 0.7 nm and a strong quantum confinement effect occurs for Cu_2O nanoparticles with a diameter less than 0.7 nm [8]. This size range is slightly smaller than the mean diameter of the Cu_2O QDs fabricated in this study. The QD size range in this case corresponds to the weak quantum confinement region. Therefore, the variation of the optical band gap is clearly due to the quantum confinement effect in the Cu_2O QDs. The Cu_2O QDs, 3.2 nm in diameter, showed absorption edge very close to the bulk band gap of Cu_2O because the size range of the QD ensemble is much larger than the exciton Bohr radius of the Cu_2O. The Cu_2O QDs, 2.9 and 3.2 nm in diameter, showed double and single distinct peaks, as indicated by the arrow in Fig. 4. The peak energies were 1.93 and 2.06 eV for the 2.9 nm Cu_2O QDs and 2.13 eV for the 3.2 nm Cu_2O QDs. These emission peak energies are smaller than the bulk band gap energy 2.17 eV of Cu_2O. The origin of these peaks is unclear, but it might be due to the formation of CuO or surface defects within the Cu_2O QDs, as reported elsewhere [8,17,18,27].

Fig. 5(a) shows the PL spectra of the Cu_2O QDs as a function of the diameter measured at room temperature for the five layered Cu_2O QDs/Al_2O_3 structures as shown in the inset of Fig. 4. The Cu_2O QDs, 3.2 nm in diameter, showed single emission peak around 550 nm, which was slightly higher than the band gap of bulk Cu_2O. As the size of the Cu_2O QDs decreases, shoulder peaks at the higher energy side develop, resulting in a broad emission spectrum. The broad PL spectrum from the 2.1 nm sized Cu_2O QD was composed of multiple elementary PL emission peaks and was deconvoluted by fitting a multiple Gaussian function, as shown in Fig. 5(b). The three elementary peaks at 416, 491 and 581 nm correspond to the Cu_2O QD ensembles with a different size distribution. During the PL emission process, electrons and holes are generated by an excitation laser and are recombined simultaneously in the potential wells with a different depth. If the energy barrier height is lower than the thermal energy for the electrical charge carriers, recombination occurs only at the deeper wells dominantly because of the charge carrier transport and redistribution process between the QDs with different sizes [28]. In this case, however, the energy barrier is much larger than the thermal energy because a large band gap material, Al_2O_3 (~8.8 eV), was used as a barrier layer between the Cu_2O QD layers. Each Cu_2O QD was isolated electrically in the Al_2O_3 matrix. This avoids the escape of the electrical charge carriers from the potential wells provided by Cu_2O QDs, which finally results in multiple PL emission peaks from the Cu_2O QDs with different size distributions.

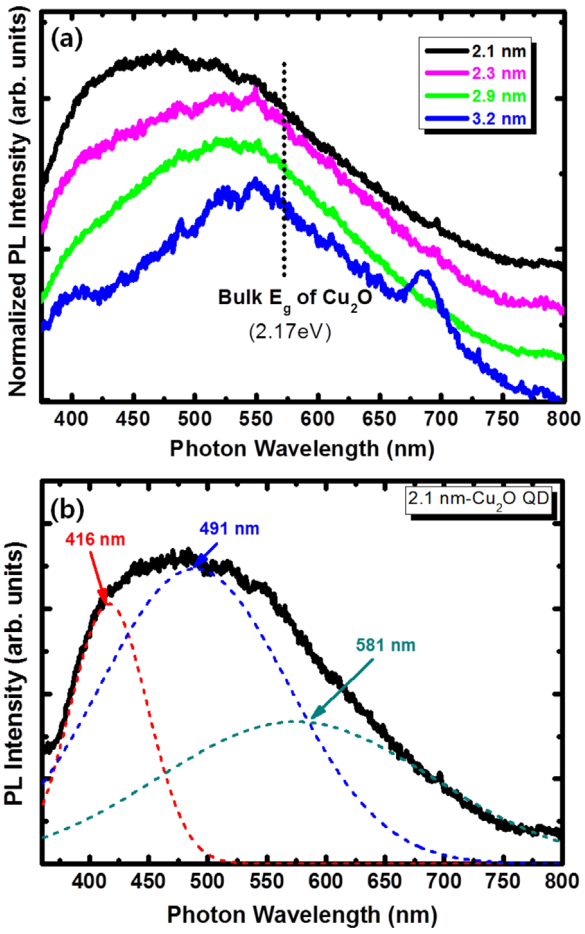

Fig. 5. (a) Normalized PL spectra measured at room temperature for Cu_2O QDs with various sizes. (b) Multiple Gaussian peaks for the deconvolution of PL spectrum are shown by the dashed lines.

4. Conclusion

Cu_2O QDs showing controlled emission due to quantum confinement were fabricated. The Cu_2O thin layers deposited by ALD showed stoichiometric Cu_2O without impurities and CuO or Cu phase. The plan-view TEM results for the ALD-grown Cu_2O revealed the formation of QDs and the density and size increased systematically with increasing number of ALD cycles, *i.e.*, the thickness of the Cu_2O layer on Al_2O_3. As the number of ALD cycles was increased from 60 to 120, 240 and 480, the diameter of the Cu_2O QDs increased from 2.1 to 2.3, 2.9 and 3.2 nm, respectively. From the initial growth behaviors of the Cu_2O islands, the growth mechanism for the Cu_2O QDs was found to be Volmer–Weber growth mode. The electron diffraction patterns of the QD areas clearly showed a spotty-pattern, indicating the successful formation of the cuprous Cu_2O QDs with a cubic structure. The absorption spectral results indicated that the electron energy transition in the Cu_2O QDs was a direct process. The optical band gaps for the Cu_2O QDs decreased from 2.71 to 2.15 eV with increasing diameter of the QDs from 2.1 to 3.2 nm due to the quantum confinement effect. The Cu_2O QDs showed broad emission peaks composed of multiple elementary peaks at 416, 491 and 581 nm, which corresponded to the Cu_2O QD ensembles with different size distributions. As the size of the Cu_2O QDs decreases, the shoulder

peaks at the higher energy side developed because their size was in the weak quantum confinement regions. These results imply that the Cu2O QDs are successfully fabricated via this method and can be a potential candidate material for optoelectronic applications.

Acknowledgments

The authors thank to Mr. Gwang-Hee Nam (Yeungnam University) for assistance with the experiments. This study was supported by the Basic Science Research Program (NRF-2014R1A2A1A11054154) and Mid-career Researcher Program (2015R1A2A2A04004945) through the National Research Foundation funded by the Ministry of Science, ICT and Future Planning of the Korean government.

References

[1] C.M. Lieber, Z.L. Wang, MRS Bull. 32 (2007) 99–108.
[2] J.H. Bang, P.V. Kamat, Adv. Funct. Mater. 20 (2010) 1970–1976.
[3] H. Weller, Adv. Mater. 5 (1993) 88–95.
[4] T.D. Krauss, F.W. Wise, D.B. Tanner, Phys. Rev. Lett. 76 (1996) 1376–1379.
[5] P. Reiss, S. Carayon, J. Bleuse, Phys. E 17 (1995) 95–96.
[6] N. Caswell, P.Y. Yu, Phys. Rev. B 25 (1982) 5519–5522.
[7] R.J. Elliot, Phys. Rev. 124 (1961) 340–345.
[8] K. Borgohain, N. Murase, S. Mahamuni, J. Appl. Phys. 92 (2002) 1292–1297.
[9] S. Ram, C. Mitra, Mater. Sci. Eng. A 304–306 (2001) 805–809.
[10] R.N. Briskman, Sol. Energy Mater. Sol. Cells 27 (1992) 361–368.
[11] B.P. Rai, Sol. Cells 25 (1988) 265–272.
[12] X. Deng, Q. Zhang, E. Zhou, C. Ji, J. Huang, M. Shao, M. Ding, X. Xu, J. Alloy. Compd. 649 (2015) 1124–1129.
[13] R. Laskowski, P. Blaha, K. Schwarz, Phys. Rev. B 67 (2003) 075102–075110.
[14] J.T. Zhang, J.F. Liu, Q. Peng, X. Wang, Y.D. Li, Chem. Mater. 18 (2006) 867–871.
[15] H. Zhu, J. Wang, G. Xu, Cryst. Growth Des. 9 (2009) 633–638.
[16] M. Yin, C.-K. Wu, Y. Lou, C. Burda, J.T. Koberstein, Y. Zhu, S. O'Brien, J. Am. Chem. Soc. 127 (2005) 9506–9511.
[17] J.A. Switzer, C.J. Hung, E.W. Bohannan, M.G. Shumsky, T.D. Golden, D.C. Van Aken, Adv. Mater. 9 (1997) 334–338.
[18] S. Banerjee, D. Chakravorty, Europhys. Lett. 52 (2000) 468–473.
[19] H. Kim, S.I. Bae, S.-H. Kim, K. Ko, H. Kim, H.-W. Kwon, J.-H. Hwang, D.-J. Lee, Appl. Surf. Sci. 349 (2015) 673–682.
[20] C. Meissner, S. Ploch, M. Pristovsek, M. Kneissl, Phys. Status Solidi C 6 (2009) S545–S548.
[21] J.C. Tauc, Optical Properties of Solids, North-Holland, Amsterdam, 1972.
[22] Y. Kayanuma, Phys. Rev. B 38 (1988) 9797–9805.
[23] L.E. Brus, IEEE J. Quantum Electron. 22 (1986) 1909–1914.
[24] J.W. Hodby, T.E. Jenkins, C. Schwab, H. Tamura, D. Trivinch, J. Phys. C 9 (1976) 1429–1439.
[25] A. Goltzene, C. Schwab, Phys. Status Solidi B 92 (1979) 483–487.
[26] C. Noguet, J. Phys. 31 (1970) 39T.
[27] Y. Chen, Y. Cao, Y. Bai, W. Yang, J. Yang, H. Jin, T. Li, J. Vac. Sci. Technol. B 15 (1997) 1442–1444.
[28] I.K. Park, M.K. Kwon, J.O. Kim, S.B. Seo, J.Y. Kim, J.H. Lim, S.J. Park, Y.S. Kim, Appl. Phys. Lett. 91 (2007) 133105.